

Impacts of Realistic Urban Heating, Part I: Spatial Variability of Mean Flow, Turbulent Exchange and Pollutant Dispersion

Negin Nazarian^{1,2}  · Alberto Martilli⁴ · Jan Kleissl³

Received: 22 February 2016 / Accepted: 26 September 2017 / Published online: 14 October 2017
© Springer Science+Business Media B.V. 2017

Abstract As urbanization progresses, more realistic methods are required to analyze the urban microclimate. However, given the complexity and computational cost of numerical models, the effects of realistic representations should be evaluated to identify the level of detail required for an accurate analysis. We consider the realistic representation of surface heating in an idealized three-dimensional urban configuration, and evaluate the spatial variability of flow statistics (mean flow and turbulent fluxes) in urban streets. Large-eddy simulations coupled with an urban energy balance model are employed, and the heating distribution of urban surfaces is parametrized using sets of horizontal and vertical Richardson numbers, characterizing thermal stratification and heating orientation with respect to the wind direction. For all studied conditions, the thermal field is strongly affected by the orientation of heating with respect to the airflow. The modification of airflow by the horizontal heating is also pronounced for strongly unstable conditions. The formation of the canyon vortices is affected by the three-dimensional heating distribution in both spanwise and streamwise street canyons, such that the secondary vortex is seen adjacent to the windward wall. For the dispersion field, however, the overall heating of urban surfaces, and more importantly, the vertical temperature gradient, dominate the distribution of concentration and the removal of pollutants from the building canyon. Accordingly, the spatial variability of concentration is not significantly affected by the detailed heating distribution. The analysis is extended to assess the effects of three-dimensional surface heating on turbulent transfer. Quadrant analysis reveals that the differential heating also affects the dominance of ejection and sweep events and the efficiency of turbulent transfer (exuberance) within the street canyon and at the roof level, while the vertical variation of these parameters is less dependent on the detailed heating of urban facets.

✉ Negin Nazarian
negin@smart.mit.edu

¹ University of California, San Diego, La Jolla, CA, USA

² Singapore-MIT Alliance for Research and Technology, Singapore, Singapore

³ Mechanical and Aerospace Engineering, University of California, San Diego, La Jolla, CA, USA

⁴ Center for Energy, Environment and Technology (CIEMAT), Madrid, Spain

Keywords Computational fluid dynamics · Pollutant dispersion · Realistic heating distribution · Three-dimensional street canyon · Turbulent transfer

1 Introduction

The study of street-canyon climate is of considerable importance since airflow and thermal characteristics directly influence urban energy, and dominate the health and comfort of urban dwellers. Hence, the characteristics of atmospheric motion and stability that govern the flow structure and pollutant removal from the street canyon should be closely examined.

Thermal forcing is one of the key elements determining urban microclimate. [Nakamura and Oke \(1988\)](#) first observed the influence of solar heating on the spatial variability of airflow and temperature in an urban canyon. Later, [Sini et al. \(1996\)](#) numerically demonstrated that thermal forcing could also influence the pollutant dispersion in the street canyon. Moreover, [Kim and Baik \(1999\)](#) showed that, in addition to the effect of heating intensity and canyon geometry (canyon height-to-width ratio), the flow structure and dispersion of pollutants markedly depend on the orientation of heat sources with respect to the airflow. Following these findings, a series of studies was performed to evaluate the effects of thermal forcing on various microclimate parameters and flow statistics. Wind-tunnel experiments ([Uehara et al. 2000](#); [Kovar-Panskus et al. 2002](#)) were used to evaluate the effect of surface-heating orientation on the mean flow within the canopy layer. Similarly, computational fluid dynamics (CFD) simulations of dispersion in urban-like geometries have been widely adopted to evaluate the effects of thermal stratification. [Kim and Baik \(2001\)](#) used a Reynolds-averaged NavierStokes model to propose five flow regimes according to the aspect ratio and surface-heating intensity. [Xie et al. \(2007\)](#) then evaluated the pollutant dispersion in a two-dimensional canyon for different geometries and heating intensities, and reported the formation of counter-rotating vortices in the windward heating case, corresponding to a zone of higher pollutant concentration in the windward corner. Formation of the secondary vortex in the two-dimensional canyon was later confirmed in a wind-tunnel experiment described by [Allegrini et al. \(2013\)](#). This study also demonstrated that the spatial distribution of turbulent kinetic energy (TKE) is dominated by the orientation of surface heating in the canyon, such that the counteracting momentum and buoyancy forcing in the windward heating case results in higher TKE in the canyon. The large-eddy simulations (LES) performed by [Cheng and Liu \(2011\)](#) and [Park et al. \(2012\)](#) also showed enhanced roof-level buoyancy-driven turbulence in unstable conditions that can enhance the pollutant removal.

The body of research has provided valuable knowledge on urban microclimate under unstable stratification. However, until recently, simplified and uniform heating of one urban surface (often the ground) was considered to represent solar heating ([Li et al. 2010](#); [Tan et al. 2015](#)), while in the three-dimensional urban environment, such uniform heating of merely one surface is unlikely. Rather, the flow and consequently the pollution removal from the street canyon are affected by the superposition of wall, roof, and ground heating. [Inagaki et al. \(2012\)](#) considered the heating of roof and ground surfaces and identified a zone of relatively high air temperature at the bottom of the leeward wall, and a zone of relatively low temperature at the top windward corner despite the heated roof, since due to the higher velocity at the roof level, the air penetrating into the cavity is relatively cooler. [Cai \(2012\)](#) further evaluated the superposition of roof and wall heating in a two-dimensional canyon and demonstrated that the addition of roof heating is, in fact, critical in the evaluation of turbulent exchange at the roof level. Several recent studies also considered the effect of three-dimensional realistic

heating, analyzing the energy balance components of urban facets (Qu et al. 2012; Nazarian and Kleissl 2015), as well as the flow and turbulence in street canyons (Yaghoobian et al. 2014; Nazarian and Kleissl 2016), and the drag coefficient of urban roughness for mesoscale parametrization (Santiago et al. 2014). The reported results confirm that the consideration of three-dimensional surface heating is critical in evaluating the flow and thermal field in the urban canyon, though another question has yet to be answered: *What is the effect of realistic heating on dispersion and turbulent transfer within the building roughness sublayer?*

Additionally, although the realistic heating of urban surfaces is gaining attention in the literature, yet there is no universal and comprehensive way of characterizing the flow in the street canyon under unstable conditions. Nazarian and Kleissl (2016) showed that the bulk Richardson number (Ri_b) gives insufficient information regarding flow characteristics, and parametrized the differential heating into directional thermal forcing defined by horizontal and vertical Richardson numbers, Ri_h and Ri_v , respectively. Here, we aim to evaluate the validity of this characterization method and answer the following questions: *Is the flow field and turbulent transfer in the street canyon more sensitive to the total surface heating (Ri_b), vertical instability inside the canyon (Ri_v), or horizontal heating of urban surfaces (Ri_h) due to solar insolation? Do thermal, flow, and dispersion fields correlate similarly with the proposed characterization method?*

To address these questions, a detailed indoor-outdoor building energy model (TUF-IOBES described in Sect. 2.1) is employed to compute heat fluxes from street and building surfaces, which are then used as boundary conditions for a parallelized large-eddy simulation model (PALM detailed in Sect. 2.2). In addition to evaluating the mean flow statistics, the analysis is extended to assess the effects of three-dimensional surface heating on the higher-order statistics of turbulent transfer using quadrant analysis (Sect. 4.2). Michioka et al. (2011) showed that pollutant removal from the canyon in neutral conditions is mainly determined by turbulent motions, and the turbulent flow statistics in urban-like configurations were previously evaluated by Coceal et al. (2006, 2007b) for neutral conditions. Coceal et al. (2007b) showed that in the aligned layout of buildings, the greatest heterogeneity of flow statistics is seen in the building canyon region (spanwise canyon between the buildings). Therefore, we focus on this region and extend the evaluation of flow statistics (including mean flow and turbulent fluxes) to realistic heating conditions (Sect. 4.2.2).

In comparison with previous studies, our model considers the transient non-uniform surface heating caused by solar insolation and inter-building shadowing (Sect. 2); characterizes surface heating into sets of non-dimensional parameters that integrate the geolocation, geometrical and surface characteristics (Sect. 3); and couples the indoor-outdoor heat transfer, turbulent flow field and passive pollution dispersion (Sect. 4). Additionally, the LES model is shown to be superior to commonly-used unsteady Reynolds-averaged Navier-Stokes (RANS) models in its representation of flow statistics and dispersion (Xie and Castro 2009; Salim et al. 2011; Gousseau et al. 2011), and therefore used for improved accuracy for analyzing the turbulent transfer within canyons. Section 5 summarizes the key results and provides conclusions and future perspectives.

2 Methods

In order to evaluate turbulence characteristics and dispersion behaviour in the street canyon, simulations are performed using the PALM model (Raasch and Schröter 2001; Letzel et al. 2008) with realistic thermal boundary conditions extracted from “temperature of urban facets

indoor-outdoor building energy simulator”, the TUF-IOBES model (Yaghoobian and Kleissl 2012). The TUF-IOBES model as well as the velocity and temperature fields calculated in the PALM model in the urban canopy have been validated by Yaghoobian and Kleissl (2012) and Park et al. (2012), respectively. Yaghoobian et al. (2014) validated the coupling method against the wind-tunnel experiment of Kovar-Panskus et al. (2002) as well the LES results of Cai (2012), and demonstrated that one-way coupling of the TUF-IOBES model with the PALM model can accurately account for the effects of the realistic temperature distribution over urban-canopy surfaces. For the present purpose, the prognostic equation for passive scalars is also solved. This component of the PALM model was successfully validated by Park et al. (2012) against the wind-tunnel data of Meroney et al. (1996) with $R^2 = 0.97$, R being the correlation coefficient. Additionally, we compared the quadrant measures obtained with LES with the direct numerical simulation (DNS) results of Coceal et al. (2007b). The shape of the joint probability density function (PDF), frequency of events, and value of exuberance were in close agreement in both cases. More details regarding the validation procedures are included in Appendix 1.

2.1 An Indoor–Outdoor Building Energy Simulator

In order to represent the realistic three-dimensional distribution of heating in urban areas, the temporally- and spatially-resolved (gridded) sensible heat boundary conditions are extracted from a detailed urban energy balance model. The TUF-IOBES model is a building-to-canopy model that simulates indoor and outdoor building surface temperatures and heat fluxes to estimate cooling/heating loads and energy use of buildings in a three-dimensional urban area. The model dynamically solves for indoor and outdoor energy processes, including the effects of real weather conditions, indoor heat sources, building and urban material properties, the composition of the building envelope (including windows and insulation), and waste heat from air-conditioning systems on urban-canopy temperature. At each timestep, the gridded energy model for exterior surfaces (Krayenhoff and Voogt 2007) is coupled with the bulk indoor model (developed based on ASHRAE Toolkit). Further information on the simulation set-up and model description can be found in Appendix 2, as well as in Krayenhoff and Voogt (2007) and Yaghoobian and Kleissl (2012).

2.2 Parallelized Large-Eddy Simulation Model

The PALM model (Raasch and Schröter 2001; Letzel et al. 2008; Maronga et al. 2015) solves the filtered incompressible Boussinesq equations, the first law of thermodynamics, the equation for subgrid-scale (SGS) TKE and the passive scalar (pollutant) equation. The numerical schemes used are the third-order RungeKutta scheme for time integration and the second-order Piacsek and Williams scheme (1970) for advection. The SGS turbulent fluxes are parametrized using a 1.5-order TKE scheme (Deardorff 1980) which uses SGS TKE to calculate eddy viscosity. A detailed description of the PALM model can be found in Letzel et al. (2008) and Maronga et al. (2015). The simulation set-up is further explained in Sect. 2.2.1 and Appendix 2.

2.2.1 Boundary Conditions and Simulation Set-Up

The schematic of the computational domain is shown in Fig. 1. All simulations are performed over a five by three array of uniformly-spaced obstacles with a canyon aspect ratio $AR = H/W = 1$, where H is the building height and W is the canyon width. The

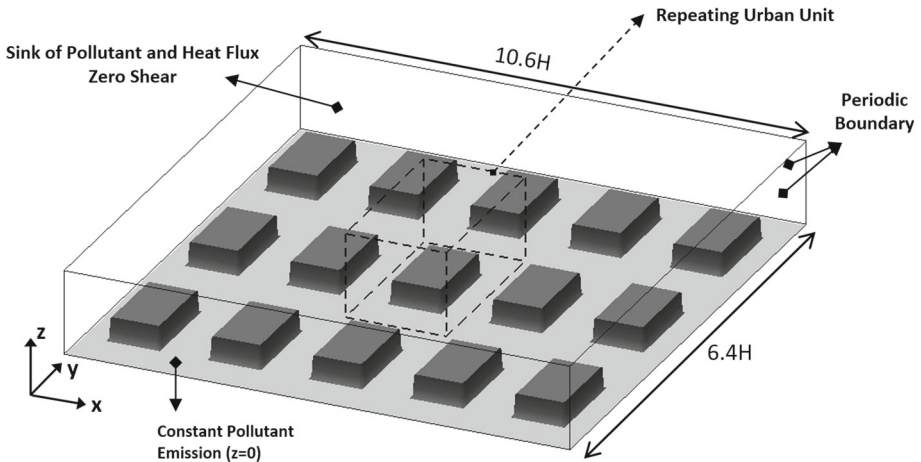


Fig. 1 Schematic of the computational domain and boundary conditions. Dashed lines represent the boundary of the repeating “urban unit” used for the results analysis

configuration represents a compact low-rise urban zone (Stewart and Oke 2012), corresponding to a roughness plan area density, $\lambda_p = A_p/A_T = 0.29$, and frontal area density, $\lambda_f = A_f/A_T = 0.25$. Here, A_p , A_f , and A_T indicate the plan area, the frontal area, and the total area of roughness elements, respectively. The canyon height is resolved by 30 grid points (grid resolution of $0.03H$), corresponding to $64 \times 64 \times 128$ grid points for each urban unit of $2H \times 2H \times 7.4H$ (highlighted in Fig. 1), and 7,864,320 grid points in the entire computational domain (15 urban units). The geometric configuration and grid resolution are chosen according to the sensitivity analyses performed by Yaghoobian et al. (2014) who compared the time- and ensemble-averaged profiles of velocity components, temperature, SGS TKE, and velocity variances with larger domains and finer grid resolutions. They found the proposed settings to be sufficient for resolving the large eddies influencing the canopy flow as well as the best compromise between accuracy and computational cost. The validity of the grid resolution and domain height is also investigated in this study by comparing the vertical profile of dispersive stress with DNS results of Coceal et al. (2006) that further endorsed these findings.

Periodic boundary conditions are used in horizontal directions, conserving mass-flow rate in the streamwise direction. Surface heat flux at each grid point from the TUF-IOBES model is available at 15-min intervals and temporally interpolated in the PALM model. Uniform and constant pollutant emission is prescribed at the ground boundary condition ($z = 0$), representing traffic emission as an area source. At the top boundary, a zero-gradient (free-slip) boundary condition is used for momentum, while a constant sink term is imposed for scalar and heat fluxes. Using this boundary condition, the integral of the concentration and temperature in the whole domain is constant in time, therefore, the ensemble average can be approximated by the time average. Additionally, above the buildings, the turbulent flux is nearly constant with height, which is a typical feature for the inertial sublayer (e.g. the upper part of the atmospheric surface layer).

The focus of our study is on unstable atmospheric stratification and the simulations are done for a temperate mid-latitude climate (Boston, Massachusetts with a latitude of 42.36° N), while the results can be expanded to various locations and time of the years using the characterization method further explained in Sect. 3. The simulation day is set to clear summer

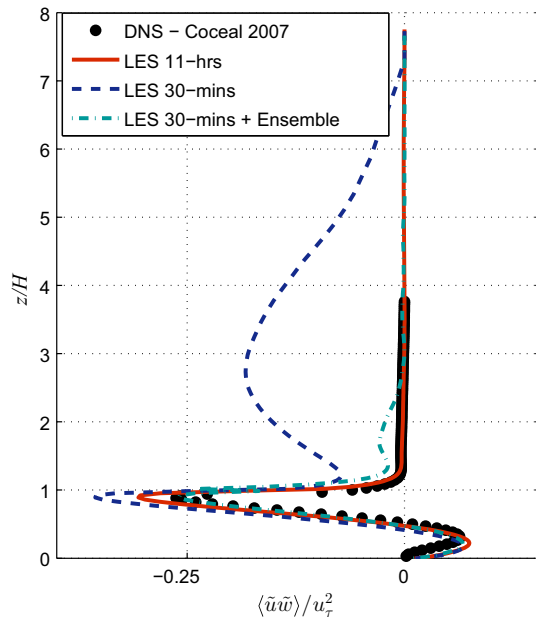
day (8 July) and the forcing data are extracted from the representative typical meteorological year (TMY3) file. Additionally, for simplicity in the future references, the volume between buildings in the spanwise canyon (along the y -axis) and streamwise canyon (along the x -axis) are referred to as “building canyon” (or “BC”), and “street canyon” (or “SC”), respectively.

2.2.2 Time-Spatial Averaging Technique

LES explicitly resolves turbulence and simulates one realization of the flow at any given timestep. For averaged quantities to be representative of the mean flow, the time-averaging interval should cover a period larger than the characteristic time scale of the turbulent fluctuations. A guiding principle is that, given the regularity of the array and the periodic boundary conditions, the time-averaged flow in each canyon must be identical. However, for a neutral simulation, 30-min averaged velocity fields shows a strong variability between canyons (Fig. 2). To ensure that this behaviour is not an artifact of the numerical settings, the choices of the domain size, grid resolution, and the horizontal boundary condition were studied but showed no influence on the variability of the results in the spanwise direction.

It is observed that this behaviour is due to the formation of roll-like circulations with axes in the streamwise direction, and the DNS analyses by Coceal et al. (2006) showed that to filter these circulations, it is necessary to average over a time period of 200–400 eddy turnover time, T , where $T = H/u_\tau$ and u_τ is the friction velocity. Coceal et al. (2006) also analyzed the so-called dispersive stress (Raupach and Shaw 1982) that accounts for the momentum transport due to time-averaged structures smaller than the size of the averaging volume, and showed that for a sufficiently large time-averaging interval, the dispersive stress should approach zero right above the canopy. In our simulations, this time interval corresponds to about 5.5–11 h. However, in the unsteady simulation of urban environments, it is not possible to use 11 h as the averaging time, since the surface heat fluxes change significantly during this time period due to the variation of solar forcing. As a compromise, we divide the computational domain

Fig. 2 Profiles of horizontally-averaged dispersive stresses ($\langle \tilde{u}\tilde{w} \rangle / u_\tau^2$) obtained using different averaging intervals, and compared with DNS results ($Re_H = 5800$) by Coceal et al. (2006). u_τ is the friction velocity over building roughness calculated based on the vertical profiles of Reynolds stresses. The overbar, $\bar{\psi}$, and bracket, $\langle \psi \rangle$, denote the time and spatial average over the horizontal plane, respectively, and $\tilde{\psi}$ represents the deviation of the time-averaged value from the time- and spatial-averaged quantity over the horizontal plane ($\tilde{\psi} = \bar{\psi} - \langle \bar{\psi} \rangle$)



into 15 urban units and combine the 30-min time average (an equivalent of $25T$), with an ensemble average of the 15 urban units (Fig. 2). The 30-min ensemble-averaged results show similar flow field in each canyon, filtering the variability in the spanwise direction, such that a small dispersive stress above the canopy is seen (Fig. 2). The simulation is then repeated for an unstable case with constant heat flux at the ground surface, and similar to the neutral case, the dispersive stresses above the canyon are reduced with ensemble averaging. Additionally, the maximum difference of ensemble-averaged velocity and temperature at each grid point are approximately 0.1 m s^{-1} and 0.2 K , when compared to the results averaged over 11 h.

3 Characterizing Momentum Versus Buoyancy Forcing

The realistic heating of surfaces in a three-dimensional urban environment is demonstrated in Fig. 3 by comparing the variation of convective heat flux (Q_h) at different urban facets. Solar noon in the simulation day is approximately at 1200 local time (eastern daylight time, EDT), which is reflected in the convective heat flux at the roof surface. Due to the ground thermal storage and the consequent increased longwave radiation exchange between ground and wall surfaces in the afternoon hours, the convective heat flux exhibits larger values after 1200 EDT at the ground and wall surfaces. Additionally, Q_h at the south wall is predominantly larger than that of the north wall, with maximum heat-flux difference occurring at 1330 EDT. These graphs demonstrate that, considering the three-dimensional and transient nature of surface heating, it is crucial that we break down the total thermal forcing on urban surfaces into directional forcing before evaluating the microclimate parameters inside the canyon.

Traditionally, the bulk Richardson number (Ri_b) is used to indicate the atmospheric stability in urban areas, where the average surface temperature of urban facets, T_s , is compared to T_a , the freestream airflow temperature. Additionally, when analyzing the microclimate of urban streets with ground heating, vertical Richardson number (Ri_v) is commonly used to indicate the atmospheric stability due to the temperature difference in the vertical direction,

$$Ri_v = \frac{gH}{U_b^2} \frac{(\overline{T_H} - \overline{T_g})}{T_a}, \tag{1}$$

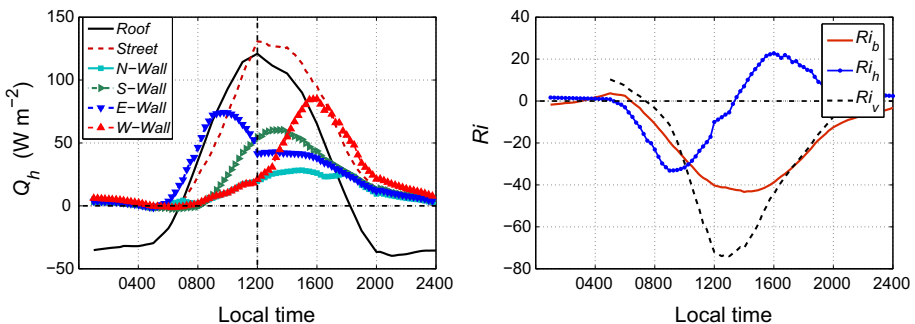


Fig. 3 Diurnal variation of convective heat flux (Q_h) averaged at different urban facets (left), and different Richardson numbers (right) for $U_b = 0.5 \text{ m s}^{-1}$. Ri_b is the bulk Richardson number calculated based on the average surface temperature of all urban facets (T_s) compared to the freestream airflow temperature (T_a), while Ri_h and Ri_v are the horizontal and vertical Richardson numbers, respectively, prescribed in Eqs. 1 and 2. U_b is the average of the streamwise component of the flow velocity that is conserved in the computation

where $g = 9.81 \text{ m s}^{-2}$ is the acceleration due to gravity, T_H is the air temperature at roof level, T_g is the temperature of the ground surface inside the building canyon, T_a is the freestream air temperature, and U_b is the bulk wind speed or the average streamwise component of the flow velocity. The definition of Ri_v avoids the use of U_H , the wind speed at building height, due to the sharp gradient of velocity at roof level that is not easily controllable (Li et al. 2010; Xie et al. 2006).

Ri_v alone neglects the horizontal temperature gradient, and falls short in a comprehensive characterization of the flow in the cross-stream canyon. Therefore, the horizontal Richardson number as defined by Nazarian and Kleissl (2016) compares the ratio between thermal forcing ($\frac{\partial F_t}{\partial x}$) and inertial forcing ($\frac{\partial F_m}{\partial z}$), in order to convey more information about the directionality of thermal forcing in relationship to the canyon vortex. In the absence of thermal forcing, the momentum forcing (F_m) inducing the vortex inside the canyon is ($\frac{\partial \overline{u'w'}}{\partial z}$). On the other hand, for a sufficiently small bulk wind speed, the thermal forcing (F_t) can be written as $g \frac{T_W - T_L}{T_a}$, where T_W and T_L are the average surface temperature of windward and leeward walls (here west and east), respectively. Therefore, horizontal Richardson number (Ri_h) can be defined by comparing the ratio of the vertical momentum and horizontal thermal forcing in the canyon, such that it indicates the effect of differential solar heating and also incorporates the effect of canyon aspect ratio H/W ,

$$Ri_h = \frac{\partial F_t / \partial x}{\partial F_m / \partial z} = \frac{gH}{U_b^2} \frac{(\overline{T_L} - \overline{T_W})}{T_a} \frac{H}{W}. \quad (2)$$

Alternatively, the horizontal Richardson number can be derived by calculating the difference between local vertical Richardson numbers adjacent to the windward and leeward walls, and scaling the difference with the canyon aspect ratio as the measure of interaction between thermal forcing of two walls and the induced canyon vortex. Accordingly, the total thermal forcing inside the canyon is divided into vertical and horizontal directional heating and their importance compared to momentum forcing is analyzed. The validity of this choice of non-dimensional quantities is analyzed through simulations with different wind speeds and surface radiative properties, but the same sets of Richardson numbers. Overall, the similarity of mean and ensemble-averaged properties is seen between two cases with the same set of Richardson numbers and the locally normalized values in two cases are shown to be very close.

3.1 Studied Cases

The bulk wind speed is varied from 0.5 to 3 m s^{-1} to span the strong to weakly unstable regimes with a wide range of vertical and horizontal Richardson numbers. Accordingly the analyses are performed for the following conditions:

- assisting condition 1, AC1 case (0900–0930 EDT), with maximum leeward heating ($Ri_h < 0$) occurring inside the canyon, i.e. minimum Ri_h and small Ri_v due to the relative roof and ground heating at this hour,
- assisting condition 2, AC2 case (1100–1130 EDT), with significant leeward and ground heating (i.e. large negative Ri_v) occurring inside the spanwise canyon,
- opposing condition, OC case (1500–1530 EDT), when large windward heating ($Ri_h > 0$) occurs combined with roof/ground heating, such that the magnitude of Ri_v and Ri_h are the same as AC2 case, while the sign of Ri_h is different (windward versus leeward heating), and

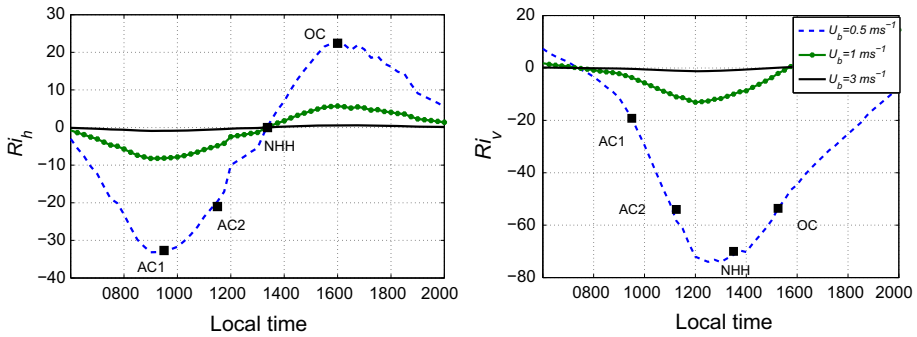


Fig. 4 Dirurnal variation of horizontal (Ri_h) and vertical (Ri_v) Richardson numbers at different wind speeds. The studied conditions prescribed in Table 1 are identified here with black squares

Table 1 Studied conditions

| $U_b = 0.5 \text{ m s}^{-1}$ Time of day (EDT) | AC1 0900–0930 | AC2 1100–1130 | NHH 1300–1330 | OC 1500–1530 |
|---|------------------|------------------|------------------|-----------------|
| $\overline{Ri_v}(BC)$ | -15.2 | -56.1 | -72.7 | -54.1 |
| $\overline{Ri_h}(BC)$ | -33.1 | -21.7 | 0 | 19.5 |
| $\overline{Ri_v}(SC)$ | -44.4 | -52.1 | -37.4 | -7.0 |
| $\overline{Ri_h}(SC)$ | -5.4 | -13.4 | -15.5 | -7.9 |

Values of Ri_h and Ri_v are averaged over the time interval of 1800 s, indicated by the overbar
 AC assisting condition, NHH no-horizontal heating, OC opposing condition, BC building canyon (spanwise), SC street canyon (streamwise)

(d) no-horizontal heating condition, NHH case (1300–1330 EDT), when both roof and ground surfaces are at maximum heating with the largest Ri_v , while Q_h values at west and east walls are the same, therefore $Ri_h = 0$.

The studied cases are demonstrated in Fig. 4 and Table 1. These choices of stability conditions allow us to evaluate and compare the effect of windward versus leeward heating (AC2 case vs OC case), as well as the importance of vertical versus horizontal temperature gradient (AC1 case vs NHH case) on the pollutant concentration and thermal field under realistic three-dimensional heating. Cai (2012) used the similar terminology of “opposing” and “assisting” conditions to characterize the flow, however, the realistic consideration of heating in our study imposes a more complex spatial distribution of surface heating. For instance, inter-building shading results in non-uniform heating of wall and ground surfaces; wall and ground surfaces in the streamwise canyons are also heated during the day; and the absolute value of Ri_v and Ri_h are slightly different when comparing the opposing and assisting conditions.

4 Results and Discussions

The results analyses are structured as follows. Firstly, the contour plots of flow, temperature, and pollutant concentration are investigated at different locations in the canyons. Additionally, turbulent fluxes of heat, momentum, and scalar are evaluated to analyze the effect of directional heating on turbulence inside the street canyon, compared with simplified cases of

uniform heating (Li et al. 2010; Cheng and Liu 2011) and two-dimensional street canyons (Tan et al. 2015). These detailed examinations in Sect. 4.1.1 further improve our understanding of the effects of three-dimensional heating orientation and intensity (quantified by Richardson numbers) on concentration distribution and the mechanisms involved in pollutant dispersion.

Secondly, the effect of surface heating on turbulent events is studied by performing a detailed quadrant analysis (Sect. 4.2). This analysis is performed at three different regions within the building roughness sublayer, identified for a neutral flow over building roughness by Coceal et al. (2007a): (1) within the building canopy, (2) shear layer at rooftop height, and (3) the rough wall flow above the building height. Quadrant analysis is an effective method for specifying the frequency of coherent structures (such as sweeps and ejections) compared to intermittent events (inward and outward interactions), and quantifying their contributions to the total turbulent transport at different positions.

Lastly, “breathability” and comfort in urban environments are analyzed by studying the pollutant concentration and exchange processes in the three-dimensional geometry, explained in detail in Part II.

4.1 Wind, Temperature, and Concentration Fields

4.1.1 Mean Flow

The contour plots of mean wind speed superimposed by velocity vectors, followed by the plots of normalized temperature and pollutant concentration are shown in Fig. 5 for cases of $U_b = 0.5$ and 3 m s^{-1} . The results are time-averaged over 1800 s and ensemble-averaged in the computational domain (Sect. 2) and reported for the *assisting* (AC1 and AC2 cases), *opposing* (OC case), and *no-horizontal heating* (NHH case) conditions, according to their Richardson numbers described in Sect. 3.1.

Following observations are made when comparing the vortex formation in the building canyon at different stability conditions. First, for the highly unstable case ($U_b = 0.5 \text{ m s}^{-1}$ and $\max(Ri_v) = -72.7$), the size of the primary vortex is larger than the height of the building; the separation and impingement of the fluid onto the top of the windward wall is more pronounced, and the formation of the secondary vortex is seen at the windward corner. When U_b is increased from 0.5 to 3 m s^{-1} , therefore decreasing Ri for the same heating distribution, the canyon vortex intensity decreases while the size expands, the centre of the vortex is moved towards the windward wall, and the region of low velocity extends deeper in the canyon. As opposed to the reported flow field in two-dimensional canyons (Tan et al. 2015; Allegrini et al. 2013), and uniform heating cases (Li et al. 2010; Cheng and Liu 2011), the region of low velocity adjacent to the windward wall is seen for all heating orientations in the three-dimensional canyon with highly unstable realistic heating ($U_b = 0.5 \text{ m s}^{-1}$). This is attributed to the heating of urban surfaces in the streamwise canyon (street canyon), and advection of flow in the building canyon from in the spanwise direction (refer to Appendix 3 for the visualization of the flow field in the spanwise direction).

When analyzing the pressure distribution in the horizontal directions (not shown), it is seen that the sign of Ri_h (i.e. the orientation of thermal forcing with respect to the wind direction) as well as the heating in the streamwise canyon significantly modify the pressure field, and consequently the flow field (Nazarian and Kleissl 2016). For instance, for the opposing condition ($Ri_h > 0$), a larger horizontal (streamwise) temperature gradient exists at the roof level, and the opposing windward heating results in higher resistance to the freestream flow. Accordingly, a lower pressure gradient is observed inside the canyon compared to the

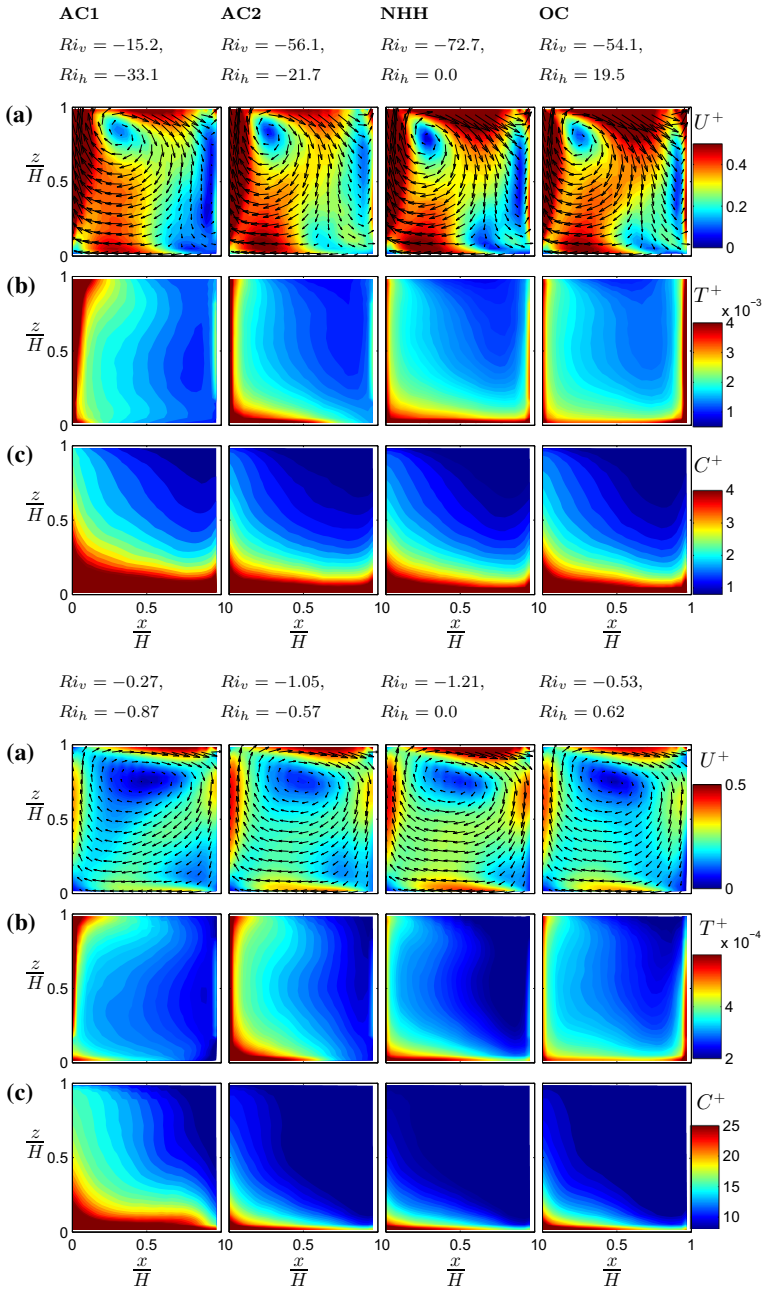


Fig. 5 Contour plots of flow properties at different studied conditions (Table 1 and Fig. 4) in the vertical plane ($x - z$) at the centre of the building canyon for $U_b = 0.5 \text{ m s}^{-1}$ (top) and 3 m s^{-1} (bottom). The first row of subplots marked with **a**, U^+ , shows the velocity magnitude $(\bar{u}^2 + \bar{v}^2 + \bar{w}^2)^{1/2}$ normalized by bulk wind speed, U_b , superimposed by velocity vectors. Following rows are the contour plots of normalized temperature ($T^+ = \frac{\bar{T} - \bar{T}_{ref}}{Q_h H / U_b}$) and concentration ($C^+ = \frac{\bar{C} - \bar{C}_{ref}}{E / U_b}$), marked by **b**, **c**, respectively, where Q_h represents total ground heat flux and E is the concentration flux. Reference height is chosen to be at $6H$. The results are time-averaged over 1800 s and ensemble-averaged according to Sect. 2.2.2

assisting conditions ($Ri_h < 0$). The horizontal pressure gradient, as well as the increased drag coefficient from the urban roughness, then result in higher momentum entering the building roughness sublayer for the opposing condition shown in Fig. 5. However, while the intensity of the canyon vortex is seemingly larger and the centre of the vortex is closer to the leeward wall, the opposing effect of buoyancy is apparent and the secondary vortex is pronounced in the windward corner of the building canyon for the highly unstable case of $U_b = 0.5 \text{ m s}^{-1}$.

For the no-horizontal heating condition (NHH case, $Ri_h = 0$), the heat advected from the ground surface produces a larger temperature increase in the canyon than the convection from the roof, therefore increasing the strength of the vortex in the building canyon. It is worth mentioning that this behaviour can be reversed when the more dominant roof heating decreases the vortex strength in the canyon (Nazarian and Kleissl 2016). Therefore the effect of roof heating should not be neglected and requires further investigation in the three-dimensional street configuration. Comparing the flow field in NHH case (strong vertical heating inside the canyon) with AC1 case (strong horizontal heating), it can be concluded that the effect of the vertical temperature gradient in increasing the intensity of canyon vortex is more dominant, and the effect of horizontal heating becomes less significant when stability is increased.

The difference between assisting and opposing conditions (AC2 and OC cases) is more pronounced in the temperature distribution, when the boundary conditions are modified directly. At assisting conditions, the elevated temperatures are only concentrated near the heated leeward wall and the heat is primarily transported vertically along the wall. In the opposing conditions, however, higher air temperature is observed within the canyon suggesting enhanced heat transfer and mixing inside the canyon. Mass flow rate is conserved in the streamwise direction (constant bulk wind speed), and the resulting temperature gradient at roof level in addition to the temperature/pressure gradient in spanwise direction are contributing to increased momentum entering the building sublayer at opposing conditions.

Subsequently, the distribution of the pollutant concentration can be explained by the vortex formation in the building canyon. The primary vortex moves the ground-level emission and the maximum of the pollutant is always concentrated at the corner of the leeward wall and ground, while there exist a second point of maximum concentration at windward corner for $U_b = 0.5 \text{ m s}^{-1}$ due to the formation of the secondary vortex. The minimum value is located at the top-east corner of the canyon. When comparing the cases with the similar magnitude of Ri_v but opposing wall heating (OC and AC2 cases), the concentration is larger for the AC2 case due to the lower intensity of the canyon vortex. However, compared to the temperature distribution, the concentration is only slightly different, indicating that unlike the thermal field, the distribution of concentration is less dependent on the horizontal temperature gradient and is more affected by the overall heating of surfaces. This behaviour is also seen in the AC1 case compared to the NHH condition. Accordingly, the no-horizontal heating condition with the maximum value of vertical Richardson number has the lowest concentration due to the enhanced mixing in the absence of wall heating in the streamwise canyon ($Ri_h = 0$). Normalized concentration increases with the decrease in vertical and horizontal Richardson numbers (increasing U_b) since the flow approaches the neutral stability conditions.

4.1.2 Turbulent Energy and Transfer

Figures 6 and 7 demonstrate the turbulent fluxes of momentum ($\overline{u'_i u'_j}$), heat ($\overline{w' T'}$), and pollutant ($\overline{w' C'}$), as well as the total TKE (\overline{k}/U_b^2) at different thermal forcing conditions. Analyses are done for the convective case ($U_b = 0.5 \text{ m s}^{-1}$) and the contour plots are out-putted for different values of Ri_h and Ri_v at the centre of building canyon ($x - z$ plane).

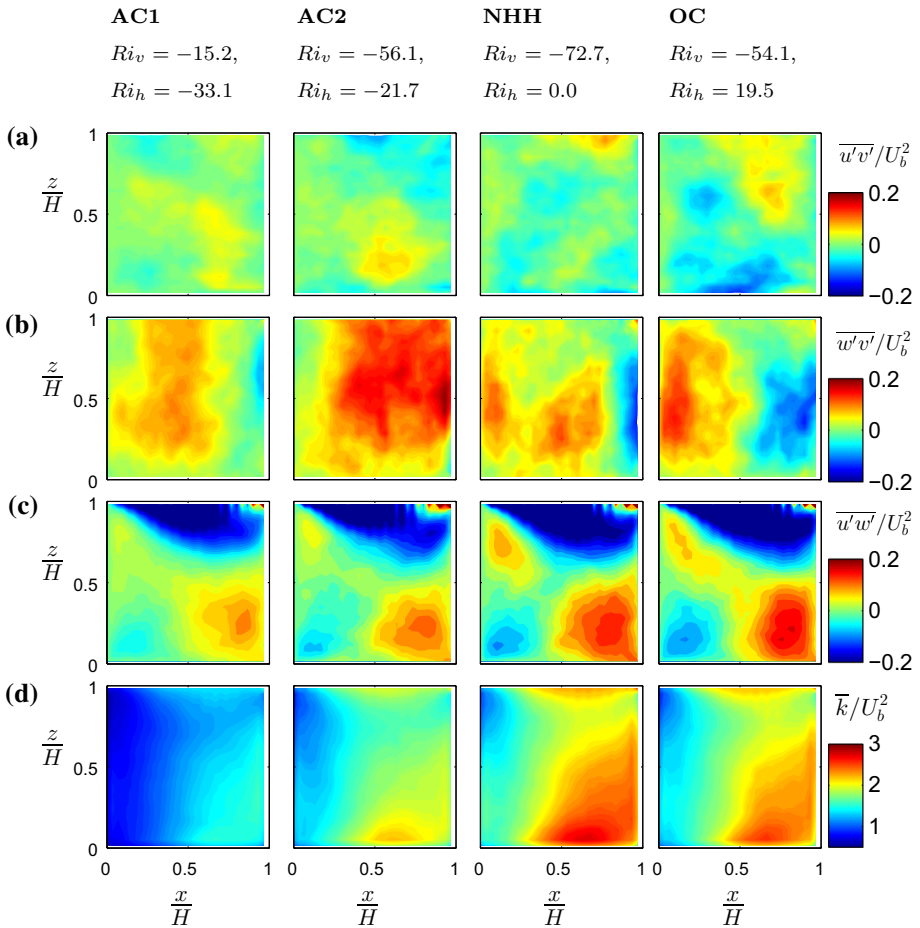


Fig. 6 Contour plots of normalized velocity covariances ($\overline{u'_i u'_j} / U_b^2$) shown in rows **a–c** and TKE (\overline{k} / U_b^2) marked as row **d** for $U_b = 0.5 \text{ m s}^{-1}$. The plane position and averaging interval are similar to Fig. 5

The results are time-averaged over 1800 s and ensemble-averaged according to Sect. 2.2.2. It can be seen that turbulent fluctuations are not entirely filtered out in the contour plots of $\overline{u'v'}$ and $\overline{w'v'}$ due to the small sampling window. Nonetheless, the combination of ensemble- and time-averaging technique was shown to capture the qualitative behaviour of turbulent structures and fluxes (indicated in Sect. 2.2.2), therefore used here for analyzing the effects of realistic heating on the turbulent transfer, as well as comparing the significance of different components of Reynolds stresses in the three-dimensional canyon.

It is evident that the turbulent momentum flux in a three-dimensional canyon is dominated by the vertical transport of the horizontal momentum ($\overline{u'w'}$ and $\overline{w'v'}$), while the horizontal Reynolds stress, $\overline{u'v'}$, exhibits a relatively small magnitude (Fig. 6). Unlike in the two-dimensional canyon, the magnitude of $\overline{w'v'}$ has a significant contribution to the vertical momentum flux, and shows sensitivity to the orientation of the surface heating. For instance, at assisting conditions, roughly uniform and positive value of $\overline{w'v'}$ is seen inside the building canyon, whereas in the no-horizontal heating and opposing conditions, a region of negative

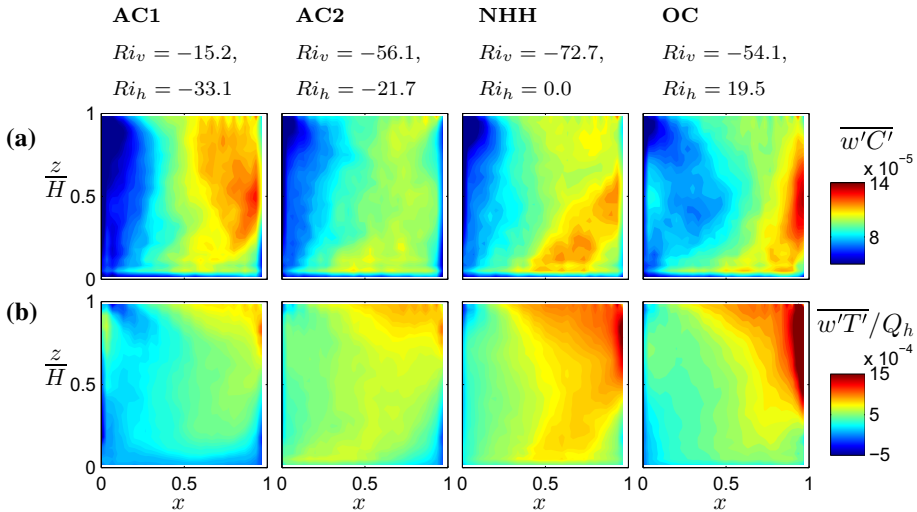


Fig. 7 Similar to Fig. 6 for time-averaged turbulent heat ($\overline{w'C'}$) and scalar ($\overline{w'T'}$) fluxes, demonstrated in rows **a**, **b**, respectively

$\overline{w'v'}$ is also observed adjacent to the leeward wall. It should be noted that, although heat flux at south and north walls are varied, the temperature differences are the same for the OC and AC2 cases. Therefore, the difference in $\overline{w'v'}$ cannot be attributed to the surface heating in the street canyon, and is directly affected by the sign of Ri_h .

At the roof level, large negative $\overline{u'w'}$ is seen for all heating conditions, that indicates a substantial exchange of mass and momentum entrainment due to the strong shear layer. Besides, the roof-level vertical momentum flux is enhanced for the no-horizontal heating and opposing conditions which is due to the increased intensity of the primary vortex. A second point of negative $\overline{u'w'}$ is seen at the leeward corner of the canyon, which was not previously observed in the two-dimensional canyons with uniform heating (Cheng and Liu 2011; Li et al. 2010). The negative vertical momentum flux can be attributed to the three-dimensional effect of the building canyon, where the mass transfer from the streamwise canyon occurs due to the counter-rotating vortices formed in the $x - y$ plane (visualization included in Appendix 3). Additionally, in the windward corner of the building canyon, positive momentum flux $\overline{u'w'}$ is observed, which is generated and enhanced due to the buoyancy-driven flow in unstable conditions. In the windward heating (OC) case with the formation of the secondary vortex, the value of $\overline{u'w'}$ in this region is significantly increased due to the opposing buoyancy effect at this condition.

For the neutral conditions, Salizzoni et al. (2009) showed that TKE values within the two-dimensional canyon are uniform except close to the windward wall and about one order of magnitude lower than those in the freestream flow. Here, when considering the thermal forcing, the large value of TKE (\overline{k}/U_b^2) adjacent to the windward wall is also seen regardless of the heating orientation, which is attributed to the shear generated by the primary canyon vortex. Additionally, it is evident that the TKE close to the ground and windward wall is markedly enhanced due to the added effect of buoyancy, and is sensitive to the orientation of the wall heating, i.e. the sign of Ri_h . Accordingly, \overline{k}/U_b^2 is the largest for the NHH case and smallest for the AC1 case. Due to the opposing effect of momentum and buoyancy forcing at the OC case, a significantly larger value of TKE is seen for the opposing condition compared

to AC2 case. It is worth mentioning that although the total TKE is dependent on both Ri_h and Ri_v , the spatial distribution of velocity variances contributing to the total TKE remains unchanged with the heating intensity and orientation (figure not shown). Additionally, unlike the two-dimensional street canyon with uniform heating reported in [Cheng and Liu \(2011\)](#), the value of $v'v'$ has the most contribution to the TKE production with the largest value at the corner of the windward wall. This is due to the modification of counter-rotating vortices by the surface heating in the street canyon, as well as the ground heating in the building canyon.

Additionally, turbulent transfer of heat and pollutant ([Fig. 7](#)) is most expressed in the vertical direction. Other components of momentum, heat, and scalar fluxes are negligible, except for the $\overline{u'T'}$ at the roof level particularly for the assisting conditions. Vertical heat and scalar transfer, $\overline{w'T'}$ and $\overline{w'C'}$, respectively, are maximum for windward heating (OC case) adjacent to the heated wall, mainly due to the increased vortex intensity and the opposing buoyancy effect for the OC case. Also, in the no-horizontal heating condition, strong positive turbulent fluxes are seen close to the ground surface.

4.2 Coherent Structures in Unstable Urban Roughness

The mean flow properties discussed in [Sect. 4.1.1](#) give insights into the turbulent flow field, but do not reveal the mechanisms involved in the turbulent exchange of momentum, heat, and pollutants at a particular height or location. Thus, for a deeper understanding regarding the modification of turbulent structures by thermal forcing in the roughness sublayer, joint PDF and quadrant measures of flux densities are analyzed in this section.

The quadrant analysis is a method of analyzing turbulent coherent structures by decomposing the joint probability of turbulent fluxes, such as Reynolds stress ($u'w'$), turbulent heat flux ($w'T'$), and turbulent scalar flux ($w'C'$), into four events (quadrants) based on the sign of the fluctuating components ([Wallace et al. 1972](#); [Willmarth and Lu 1972](#); [Antonia 1981](#)). For instance, when analyzing the vertical momentum transport ($u'w'$), the events in quadrant 2 and 4 ($u'w' < 0$) are called ejections and sweeps, respectively, and indicate the organized events that contribute positively to the downward momentum flux. Events in quadrant 1 and 3 ($u'w' > 0$) are called outward and inward interaction, respectively, and represent the unorganized counter-flux events. Therefore, the shape of a joint PDF gives information on the importance of ejections and sweeps, intermittency of turbulence, and the efficiency of fluxes.

Additional information on the turbulent exchange processes can be obtained from the probability density function and quadrant analysis. The time fraction of an event i , E_i , which is the relative total duration of events in quadrant i , can be calculated for any two parameters a and b as

$$E_i = \int_{l_a}^{u_a} \int_{l_b}^{u_b} P(a, b) da db, \quad (3)$$

with $\sum_{i=1}^4 E_i = 1$ where $P(a, b)$ is the joint PDF of a and b , and the lower and upper integration limits are defined based on the flux density. For instance, typically $u'w'$ is directed towards the surface while all other flux densities transport mass or energy away from the surface. Therefore, the numbering of quadrants is arranged such that the mean vertical wind gradient is opposite to the mean vertical temperature and concentration gradient [refer to [Christen et al. \(2007\)](#) for detailed integral limits based on the desired a and b]. The contribution of each quadrant to the total flux density can be computed as the flux (or stress) fraction, S_i , introduced by [Raupach and Thom \(1981\)](#) as

$$S_i = \frac{1}{r_{ab}} \int_{l_a}^{u_a} \int_{l_b}^{u_b} abP(a, b)da db, \quad (4)$$

with $\sum_{i=1}^4 S_i = 1$ where r_{ab} is the correlation coefficient. From the stress fraction, two other measures of coherent structures can be obtained: the dominance of ejections or sweeps as S_2/S_4 ; and the exuberance (Shaw et al. 1983), which is the contribution of unorganized counter fluxes compared to the organized events in the direction of the average flux, $(S_1 + S_3)/(S_2 + S_4)$. Exuberance is regarded as the measure of efficiency for turbulent exchange.

The quadrant analysis covers the four studied conditions described in Sect. 3, and joint PDF of vertical fluxes (combinations of w with u , C and T) are calculated. Six different heights are chosen in the urban roughness sublayer up to $6H$, while 5 positions along the roof level are analyzed. Instead of using the diurnal flow simulations, each case is run in steady state and flow properties are sampled every 3 s for a period of 8 h. The joint probability density functions are calculated with 30×30 bins for \hat{u}_i , \hat{C} , and \hat{T} , where \hat{a} represents the fluctuation parameter a' , normalized by its variance, σ_a , such that $\hat{a} = a'/\sigma_a$. \hat{u}_i , \hat{C} , and \hat{T} range from -4 to 4 .

4.2.1 Quadrant Analysis in Neutral Condition

In the neutral case, $\overline{u'w'}$ is towards the surface (negative) at all studied locations, except adjacent to the windward wall. In the street canyon, u and w are nearly uncorrelated, reflected in exuberance (Exu) close to -1 , as well as the symmetric shape of the joint PDF (refer to Appendix 1 for a comparison with the DNS). Along the roof level, however, joint PDFs are highly variable. Close to the leeward wall, r_{uw} is small ($\overline{u'w'} \approx 0$) and the quadrant has a symmetric shape, with low efficiency of turbulent momentum exchange. In the centre of the canyon where the highest efficiency of turbulent momentum transfer occurs, the quadrant shape is seen as well. However, the quadrant shape is reversed and extended towards the unorganized counter-flux events adjacent to the windward wall, and $\text{Exu} \approx -2$ indicates twice as many unorganized events as the coherent structures. This can be attributed to the point of flow separation and impingement at the edge of the windward wall. Sweep events have a large contribution to the total turbulent momentum transfer at the roof level, while the transition to an ejection-dominated flow occurs above the building height. At $z/H = 1.5$, a distinct quadrant shape is observed with a higher frequency of organized events up to $3H$ and Exu converges to approximately -0.3 at around $2H$. These results are consistent with the DNS results of Coceal et al. (2007a) described in Appendix 1, as well as the measurements of Christen et al. (2007) over the urban roughness.

4.2.2 Quadrant Analysis in Unstable Conditions

Here the effects of realistic thermal forcing on transfer processes in and above the three-dimensional canyon are analyzed, and the profiles of turbulent fluxes (Fig. 8), joint PDF (Fig. 9), and quadrant measures (Figs. 10, 11) of turbulent momentum, heat, and pollutant fluxes are discussed.

Figure 8 presents profiles of turbulent fluxes with height (z) and along the roof level (x). Overall, $\overline{u'w'}$ has a small upward (positive) value at the street level, followed by the maximum downward momentum flux at the roof level, and then decreases with z reaching zero at $6H$ (the height of the computational domain is $7.5H$). Compared to the neutral case, the value of Reynolds stress $\overline{u'w'}$ is significantly enhanced due to the buoyancy effect induced by the surface heating, and is largest for the opposing heating condition. Similarly,

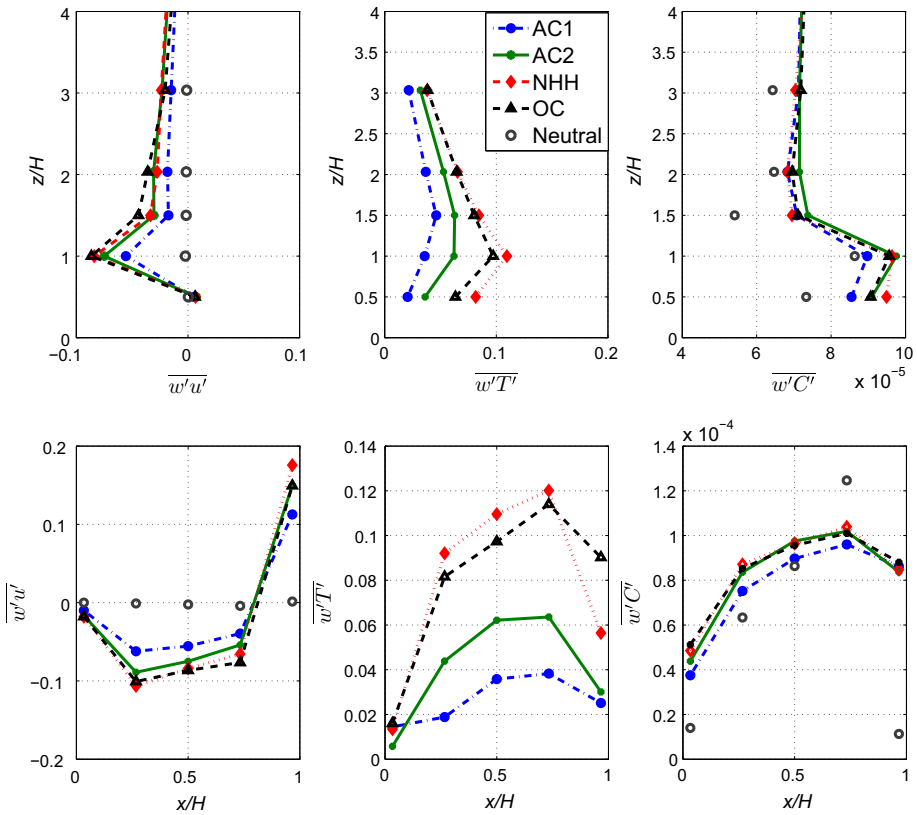


Fig. 8 Profiles of mean turbulent fluxes of momentum ($\overline{w'u'}$), heat ($\overline{w'T'}$), and scalar ($\overline{w'C'}$) with height (z), and along the roof level (x) for $U_b = 0.5 \text{ m s}^{-1}$

the turbulent vertical transport of pollutants ($\overline{w'C'}$) is enhanced with thermal forcing inside the canyon. The effect of surface heating in the canyon is apparent for all profiles, although the highest sensitivity to the heating orientation is seen for turbulent heat flux, where $\overline{w'T'}$ is the highest for the NHH case, and the opposing heating condition (OC case) exhibits significantly larger turbulent heat flux than the symmetrically opposed leeward heating (AC2 case) due to enhanced mixing in the canyon.

The direction of turbulent heat and pollutant flux is generally upward as also demonstrated by the positive value of $\overline{w'T'}$ and $\overline{w'C'}$ in Fig. 8. Therefore, for consistency in the physical interpretation of the quadrant analysis, from hereinafter the warm (high-concentration) upward moving eddies are labeled as quadrant 2, while cool (low-concentration) downward moving eddies are quadrant 4, analogous to ejections and sweeps, respectively.

Joint Probability Density Functions and Time Fractions of Quadrants. At the street level (joint PDF not shown), the correlation between u' and w' is small, and the joint PDFs are characterized by a nearly rotational symmetric shape that is similar to the neutral case. Regardless of the heating distribution, the time fraction of quadrants shows a slight dominance of unorganized events, where inward interactions (E_3) are significantly more frequent. Contrary to $u'w'$, w and T are correlated at the street level, with a higher frequency of organized events at all heating conditions. The frequency of inward interactions (E_3) is the lowest among all

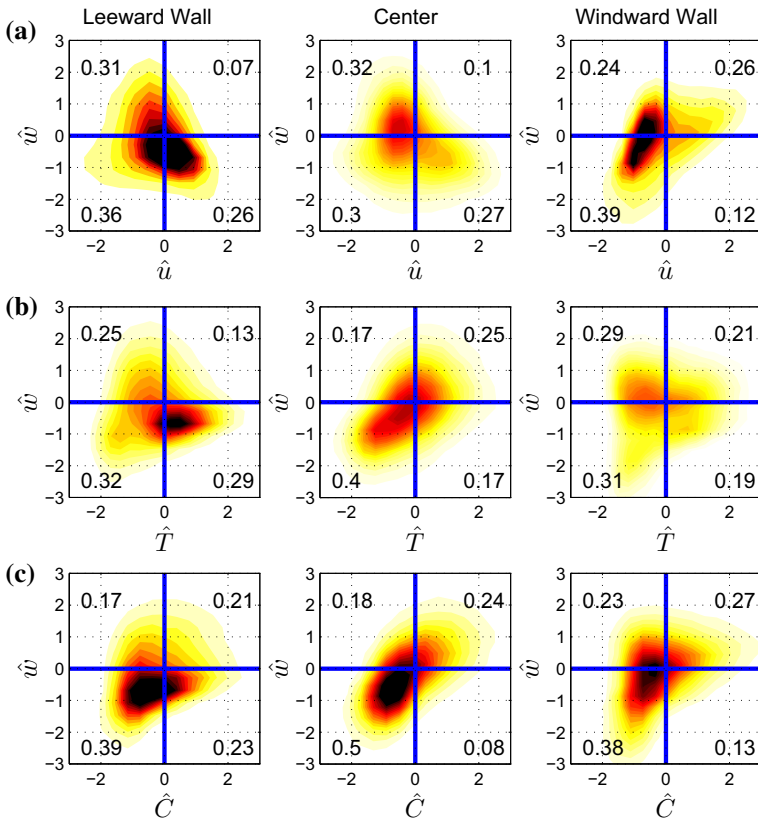


Fig. 9 Normalized joint PDF of turbulent momentum flux ($u'w'$) shown in row **a**, heat flux ($w'T'$) in row **b**, and scalar flux ($w'C'$) in row **c** at different points in the building canyon along the roof level ($z/H = 1$) for the opposing condition (OC case) at $U_b = 0.5 \text{ m s}^{-1}$. The number labelling the individual quadrants denotes the time fraction of each event (E_i) not to be mistaken for the stress fraction (S_i)

quadrants, while the fourth quadrant (cool downward-moving eddies) dominates with a slight variation based on the heating orientation. Similar to the joint PDF of turbulent heat flux, w and C are strongly correlated in the street canyon, and the frequency of organized events is significantly higher ($E_2 + E_4 \gg E_1 + E_3$) for all heating conditions. However, note that the time fraction of events (E_i) does not necessarily correlate with their contributions to the total flux (S_i).

At the *roof level* in the centre of the building canyon, r_{uw} increases, and a quadratic shape is observed with a strong dominance of organized events (Fig. 9 demonstrates an example for the opposing condition). Similar to the neutral case, high variability of joint PDF is seen along the roof level for all heating conditions. However, as opposed to the neutral case, a significant correlation is seen between u and w adjacent to the leeward wall where the quadrant shape is extended into the second and fourth quadrants and organized structures are more frequent. On the other hand, adjacent to the windward wall, the highest frequency of unorganized events is seen for all heating conditions. The high variability of joint PDF along the roof level is also apparent for $w'T'$, however, contrary to $u'w'$, the organized events are more frequent close to the windward wall ($E_2 + E_4 > E_1 + E_3$). For turbulent pollutant transport, the quadrant

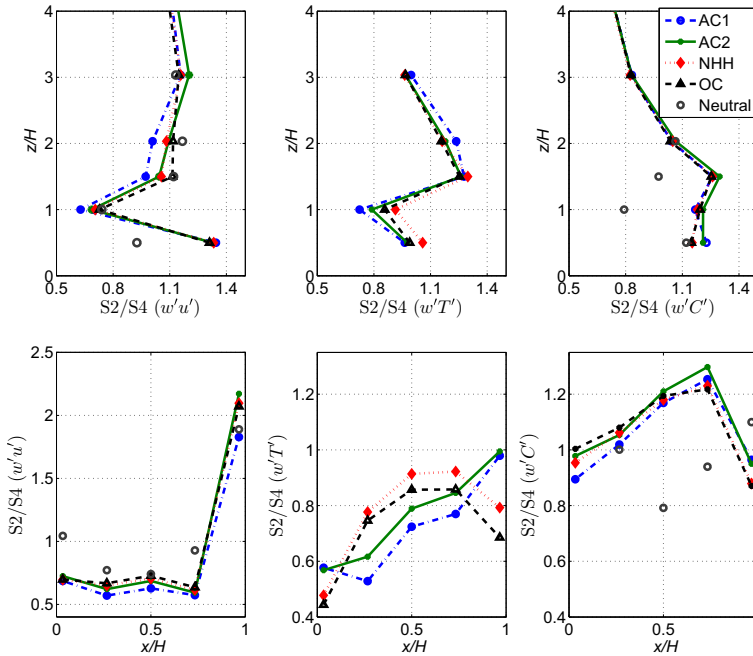


Fig. 10 Profiles of S_2/S_4 for turbulent momentum ($u'w'$), heat ($w'T'$), and scalar ($w'C'$) fluxes with height (z), and along the roof level (x) for $U_b = 0.5 \text{ m s}^{-1}$

shape is extended to the second and fourth quadrants at all locations along the x -axis at the roof level, with the lowest frequency of unorganized events at the centre.

Above the building height, the frequency of organized events becomes smaller for momentum transport, and the correlation between u and w decreases such that at $z = 2H$, the frequency of all quadrants is similar. This behaviour is different from the neutral case for momentum and from the turbulent heat and pollutant fluxes at unstable conditions, where the quadrant shape is still seen and organized events are dominant at this height.

Dominance of Ejections and Sweeps. Surface heating inside the canyon induces ejections with a large contribution to the momentum and pollutant flux density (Fig. 10) close to the surface. Accordingly, as opposed to the neutral case, the contribution of ejections to the turbulent momentum transfer is the largest at the street level for all heating orientations. For the turbulent heat flux, however, the contribution of second and fourth quadrants are the same at the centre height of the canyon (except for slight S_2 dominance for the NHH case), although the fourth quadrant (cool downward moving eddies) is more frequent. This behaviour is attributed to the three-dimensional flow structure, since the measurement of Christen et al. (2007) in a two-dimensional canyon showed quadrant 4 to be dominant for turbulent heat flux inside the canyon. Similarly, the cross over to a sweep-dominated flow ($S_2/S_4 = 1$) inside the canyon for $u'w'$ occurs close to the roof level, as opposed to the centre height of the two-dimensional canyon (Christen et al. 2007), which is consistent with the flow modification due to the three-dimensional configuration discussed in Sect. 4.1.1.

At the centre of the roof level, similar to the neutral case and the observation of the two-dimensional canyon, both turbulent momentum and heat transfer are dominated by the fourth quadrant (sweeps), however, $w'C'$ remains dominated by the second quadrant (ejections).

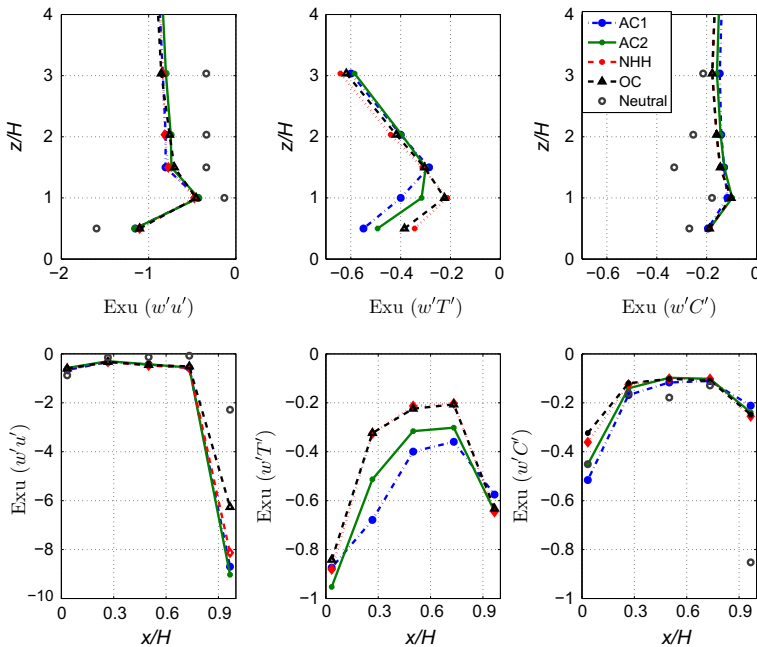


Fig. 11 Profiles of $Exu = (S_1 + S_3)/(S_2 + S_4)$ for turbulent momentum ($w'u'$), heat ($w'T'$), and scalar ($w'C'$) fluxes with height (z), and along the roof level (x) for $U_b = 0.5 \text{ m s}^{-1}$

Variability of S_2/S_4 is seen along the x axis at the roof level. Close to the windward wall, $w'u'$ transitions to a strong ejection dominated regime, and $w'C'$ crosses over to a slight domination of the fourth quadrant close to both walls ($S_2/S_4 < 1$). On the contrary, the fourth quadrant dominates the turbulent heat transfer along the x axis at the roof level, and only the orientation of heating modifies the relative importance of S_2 and S_4 (more heating induces higher S_2).

Above the building height, the turbulent transfer is dominated by ejections (quadrant 2) for all parameters, while the transition height differs for momentum and heat flux ($z/H = 1.2$ and 1.5 m , respectively), and is also lower than the two-dimensional canyon (Christen et al. 2007). Pollutant transfer is ejection-dominated up to $2H$ and transitions to sweep-dominated above.

Efficiency of Turbulent Transfer: Compared to the neutral case, the efficiency of the turbulent momentum transfer is higher at the street level, and smaller at and above the building height (Fig. 11). In other words, surface heating increases the contribution of organized structures inside the canyon, while adding more intermittency to the flow above the building height, as observed in the measurements of the two-dimensional canyon. Additionally, for all studied heating conditions at all heights, the efficiency of the turbulent pollutant exchange is significantly higher than for heat and momentum transfer. The highest efficiency of exchange for all fluxes is seen at the centre of the roof level, whereas in the measurements by Christen et al. (2007), the minimum value of Exu was located slightly higher than the roof level. This is attributed to the variation of roof shapes in real configurations which is not included in our simulations, as opposed to the difference in the two-dimensional versus three-dimensional configuration.

The sensitivity of Exu to the heating orientation is seen only for the turbulent heat transfer, and up to $z/H = 1.5$. The lowest magnitude of Exu (indicative of the highest efficiency of turbulent transfer) for $w'T'$ is seen for the NHH and OC cases, and the assisting condition 1 (with a large horizontal temperature difference) exhibits the lowest efficiency of turbulent heat transfer, specifically at the street level. The variation in Exu of the turbulent heat flux is more distinct at the roof level, where adjacent to the windward and leeward walls, the magnitude of Exu increases significantly. Similarly, at the roof level adjacent to the windward wall where the flow separation and impingement occurs, the lowest efficiency of turbulent momentum transfer is seen due to the increased intermittency. In other words, the minimum efficiency of the turbulent heat and pollutant transfer occurs at the leeward corner of the roof level, while for the turbulent momentum flux, minimum efficiency (largest magnitude of Exu) occurs at the windward corner due to the flow separation.

5 Summary and Conclusions

It is undisputed that numerical modelling of urban flow provides information on the thermal comfort, ventilation, and air quality in urban environments. However, the complexity of real-world processes limits current numerical models to certain simplifications and assumptions. These assumptions, and their validity for the accurate representation of urban microclimate, depend on the parameters and scale of interest.

At the microscale, one of the common simplifications in modelling relates to the urban morphology: idealized configurations of two-dimensional or three-dimensional street canyons are often used to represent urban areas in order to remove the uncertainty caused by complex (and random) geometries. Another common assumption relates to the urban heating: surface heating is either neglected, or uniform heating of one building facades is considered. In the current study, we aimed to elaborate on these choices by comparing (a) a three-dimensional configuration as opposed to two-dimensional canyons, and (b) realistic heating in contrast to uniform heating of one urban surface. We performed a series of large-eddy simulation runs for an idealized three-dimensional configuration (representing a compact mid-rise urban area), where unstable atmospheric stratification with ground-level pollutant emission was considered. The parameters of interest were (a) mean flow (wind, thermal, and pollutant concentration fields), (b) turbulent energy and fluxes, and (c) transport processes; and the scale of interest was the urban roughness sublayer as it hosts the majority of human activities. Additionally, we characterized the differential heating of the urban facets using sets of horizontal and vertical Richardson numbers introduced by [Nazarian and Kleissl \(2016\)](#), such that the results can be extended to further scenarios. The following is a summary of the main conclusions.

5.1 Mean Flow, Temperature, and Concentration Fields

The effect of three-dimensional configuration and realistic heating on the mean flow is highly dependent on the parameter of interest. When analyzing the *thermal field* in the urban sublayer, considering the three-dimensional heating of urban surfaces is crucial: the effect of the horizontal temperature gradient (in both intensity and orientation) is projected in the spatial distribution of temperature. Additionally, a realistic distribution of surface heating plays a pivotal role for thermal comfort and heating/cooling loads in urban areas.

In the case of the urban *flow field*, the instability level motivates or demotivates the detailed consideration of realistic surface heating, as also observed for the effect of realistic heating on

the drag coefficient (Santiago et al. 2014). For instance, the formation of the secondary vortex in the opposing condition is only seen for the highly unstable regime; while in the weakly unstable condition, the modification of the primary vortex due to the horizontal heating is less significant. Nonetheless, the roof heating, and therefore the advection of the warm air inside the building canyon, should not be neglected as it modifies the vertical instability inside the building canyon, as well as the pressure gradient in the spanwise direction. On the other hand, substantial modification of the flow field is observed for three-dimensional versus two-dimensional configurations. In the spanwise direction, modification of the flow due to the combined effect of three-dimensional configuration and heating distribution is pronounced, where the formation of counter-rotating and asymmetric vortices in and above the canyon are seen.

Lastly, when the *concentration field* is analyzed, the choice of detailed three-dimensional heating appears to be superfluous. Compared to the wind flow and thermal field, the distribution of concentration is less dependent on the horizontal temperature gradient, and is more affected by the overall heating of surfaces. Additionally, regardless of the heating orientation, the maximum concentration inside the building canyon always occurs adjacent to the leeward wall when $H/W = 1$, resulting in persistent pedestrian exposure to air pollution at this location. It is worth mentioning that this location also experiences the peak of temperature inside the canyon throughout the day. Therefore, selecting such locations for long-term outdoor activities can be harmful to human health and comfort.

5.2 Turbulent Kinetic Energy and Turbulent Transfer

The distribution and magnitude of total TKE in the building canyon are highly dependent on the realistic surface heating, while the contribution of velocity variances to TKE remains unchanged with the heating intensity and orientation.

As opposed to the two-dimensional canyons, $\overline{v'v'}$ contributes the most to the TKE in the building canyon, and $\overline{w'v'}$ is significant in the turbulent momentum transfer in the three-dimensional configuration. Similar to the two-dimensional configuration, the turbulent vertical transport of scalar ($\overline{w'C'}$) and heat ($\overline{w'T'}$) are dominant in the three-dimensional configuration, and other terms can be neglected.

5.3 Quadrant Measures and Transport Processes

The efficiency of turbulent momentum and scalar transport, identified by *exuberance* in the quadrant analysis, depends mostly on overall atmospheric instability, and less on the detailed heating distribution among urban facets. Compared to the neutral case, the efficiency of turbulent transfer is increased for $\overline{w'C'}$ and decreased for $\overline{u'w'}$. For turbulent heat transfer, however, exuberance is modified by the heating orientation, with no-horizontal heating and opposing conditions having the highest efficiency. For a more comprehensive analysis of the coherent structures in the urban roughness sublayer, quadrant measures will be supplemented in future work with a more detailed analysis of instantaneous flow as well as other statistical methods including the integral length and time scales.

The detailed LES of urban microclimate provide valuable insights into the mean flow characteristics, turbulent kinetic energy, and exchange processes within the urban roughness sublayer; and the presented results are of particular importance for urban flow and dispersion modelling. Additionally, current simulation results can be further explored to link the urban design to microscale climate, as well as human health and comfort. An example of these implications is presented in Part II.

Acknowledgements We thank Omduth Coceal from University of Reading for providing the data of the DNS analysis used in this paper. Funding was received from the National Science Foundation, Environmental Sustainability CAREER award number CBET-0847054, as well as from the National Research Foundation Singapore under its Campus for Research Excellence and Technological Enterprise programme.

Appendix 1: Supplementary Information on Model Validation

The energy balance model (TUF-IOBES) by Yaghoobian and Kleissl (2012) was validated by comparing the change of modelled interior wall temperature in response to a step change in outside air temperature with an analytical solution as well as other models. The difference between the analytical solution and the TUF-IOBES model was less than 2.3% which was lower than other numerical models, including the 5% difference reported for the CBS-MASS model (Zmeureanu et al. 1987).

The PALM model for unstable flow in the urban canopy was validated by Park et al. (2012) against the wind-tunnel measurements of Uehara et al. (2000). The agreement in the vertical profiles of the normalized streamwise horizontal velocity and temperature supported the validity of the temperature wall function in the PALM model. The normalized scalar concentration simulated using the PALM model was successfully validated against wind-tunnel data of Meroney et al. (1996) with $R^2 = 0.97$.

The coupling of the TUF-IOBES and PALM models was validated against data from the wind-tunnel experiment of Kovar-Panskus et al. (2002) for a two-dimensional street canyon with a heated windward wall, and also compared with the LES results of Cai (2012). Both numerical studies showed that based on mass conservation (downward mass flux into the canyon near the windward wall equals the upward mass flux out of the canyon near the leeward wall) the primary vortex should be shifted to the right which is different from the sketch provided by Kovar-Panskus et al. (2002) and rendered this portion of the experimental data questionable. The agreement with the Cai (2012) numerical simulation is encouraging.

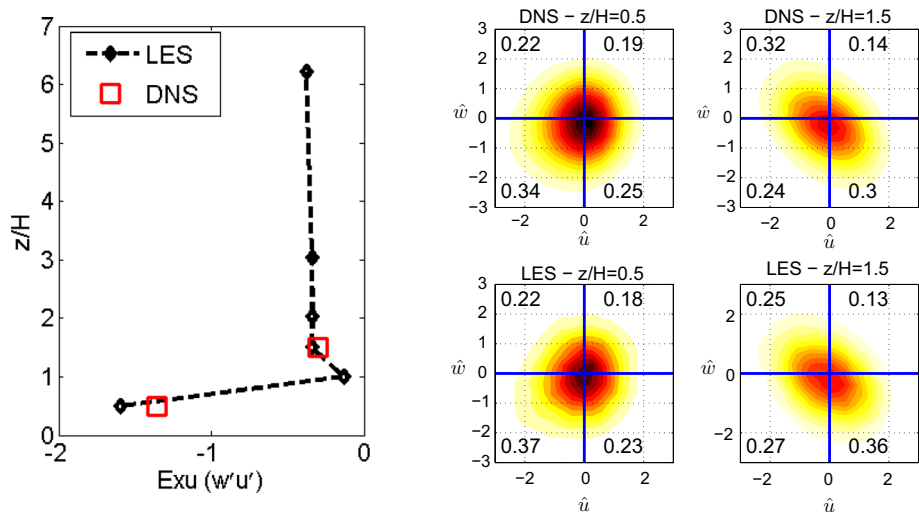


Fig. 12 Left: vertical profile of exuberance [$Exu = (S_1 + S_3)/(S_2 + S_4)$]. Right: joint probability density functions calculated for current LES results and compared with the DNS of Coceal et al. (2007a) for neutral conditions

Here, the quadrant analysis obtained by LES are compared with DNS of aligned arrays of cubes at $Re_H = 5800$ for a neutral case performed by [Coceal et al. \(2007a\)](#). The DNS data are gathered every 0.005 s at heights $0.5H$ and $1.5H$ for $100T$, where $T = H/u_\tau$, and u_τ is the friction velocity. LES results are outputted at various locations every 3 s for a period of 8 h, therefore the number of data points are similar for the comparison. Grid resolutions relative to H are similar with 32 and 30 grid points per H for DNS and LES runs, respectively. [Figure 12](#) shows close agreement in the shape of the quadrants, the frequency of events, as well as the value of exuberance at heights $0.5H$ and $1.5H$ at the centre of the canyon.

Appendix 2: Supplementary Information on Simulation Set-Up

This section describes the simulation set-up in more detail. Radiative and material properties of urban surfaces are shown in [Table 2](#), which represents an example of a typical post-1980 building in a compact low-rise zone, with painted walls and roof, and asphalt/dry-soil street covers. The physical building set-up and thermal properties are chosen similar to [Yaghoobian and Kleissl \(2012\)](#) based on the construction materials that satisfy insulation requirements for non-residential buildings in ASHRAE 90.1-2004 ([ASHRAE 2004](#)). Buildings have square footprints of $21.3 \times 21.3 \text{ m}^2$, and each wall of the buildings has a window centred on the wall with dimensions of $12.2(\text{height}) \times 15.2(\text{width}) \text{ m}^2$, resulting in a window fraction of 0.47. Total domain height is $7.4H$, where H is the building height (18.3 m).

In the TUF-IOBES model, the outdoor surface energy balance consists of net longwave radiation, L_{net} , net shortwave radiation, S_{net} (accounting for multiple reflections of direct solar radiation and shading), conduction, Q_c , and convection, Q_h , that are solved and enforced for each outdoor patch surface. Latent heat fluxes are assumed to be zero. Direct and diffuse horizontal solar radiation is based on the TMY3 forcing data. Downwelling longwave radiation from the sky is based on Browns sky model ([1997](#)) as implemented in the ASHRAE Toolkit ([2001](#)), where L_{net} is a function of the air and dew point temperatures, cloud cover, and cloud height. The transient heat conduction is solved based on the z-transform method utilizing conduction transfer functions, and the diffusion equation by [Hillel \(1982\)](#) is solved to obtain a sinusoidal temperature boundary condition at the surface with a constant temperature boundary condition at soil depth. The surface convective heat fluxes are simulated based on the temperature differences between surfaces and canopy air, multiplied by a convective heat transfer coefficient based on an empirical model known as the DOE-2 method. Further information on the model, including fenestration model and forcing data can be found in [Yaghoobian and Kleissl \(2012\)](#) and [Krayenhoff and Voogt \(2007\)](#).

Table 2 Surface radiative and material properties

| Surface | Roof | Ground | Walls |
|----------------------|------|--------|-------|
| Albedo | 0.6 | 0.1 | 0.3 |
| Emissivity | 0.9 | 0.95 | 0.9 |
| Roughness length (m) | 0.01 | 0.01 | 0.01 |

For more details on the building material thickness and thermal properties of layers refer to [Yaghoobian and Kleissl \(2012\)](#)

Appendix 3: Supplementary Analysis on the Three-Dimensional Flow Field

The effect of three-dimensional configuration and realistic surface heating in the streamwise canyon can be better understood by investigating the flow in the spanwise direction. In the absence of surface heating, several factors distinguish the roughness flow in three-dimensional aligned arrays compared to two-dimensional street canyons (Coceal et al. 2007a): (1) In the building canyon (BC, $z < H$), formation of two symmetric counter-rotating vortices is seen in the $x - y$ plane where the vortex size and its centre varies with height. (2) Due to the structure of counter-rotating vortices, the canyon vortex in the $x - z$ plane is smaller and the centre of the vortex is moved upward compared to the mid-height position in two-dimensional canyons (also shown in Fig. 5). (3) Due to the canopy-top shear layer, small eddies are shed off at the building edge into the streamwise canyon and above the building height.

The presence of surface heating further modifies the flow structure. For brevity, only the opposing condition is discussed here for different stability levels (Fig. 13). In the near-neutral case of $U_b = 3 \text{ m s}^{-1}$, the size of two counter-rotating vortices in the $x - y$ plane is as large as the canyon width, although their symmetry is influenced (indicated by the increased momentum entering the canyon from the south) by the temperature difference between north and south walls in the street canyon. In the highly unstable case, however, the two counter-rotating vortices in the $x - y$ plane shrink and occupy only half of the street-canyon region close to the leeward wall, and the vortex shed off at the building edge to the streamwise canyon is increased. This is due to the formation of the secondary vortex adjacent to the windward wall, and the increased velocity gradient at the edges of the building canyon. Additionally, the ground heating at the street canyon forces more flow in the building canyon, and enhances downward velocity in the $y - z$ plane for $U_b = 0.5 \text{ m s}^{-1}$. Subsequently, the region of low momentum above the building height is more pronounced for the opposing condition (not shown). Both temperature and concentration fields are modified by the flow structure in the building canyon and higher values are seen compared to the street canyon. T^+ and C^+ are more concentrated close to the ground and the leeward wall, and asymmetry due to differential heating in the street canyon is seen in the $x - y$ plane.

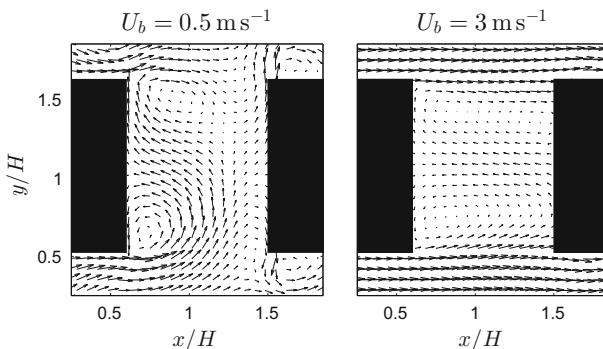


Fig. 13 Velocity vectors in the $x - y$ plane at different wind speeds ($U_b = 0.5$ and 3 m s^{-1}) for the opposing condition (OC case)

References

- Allegrini J, Dorer V, Carmeliet J (2013) Wind tunnel measurements of buoyant flows in street canyons. *Build Environ* 59:315–326
- Antonia R (1981) Conditional sampling in turbulence measurement. *Annu Rev Fluid Mech* 13(1):131–156
- ASHRAE AS (2004) Standard 90.1-2004, energy standard for buildings except low rise residential buildings. American Society of Heating, Refrigerating and Air-Conditioning Engineers, Inc., New York
- Brown DF (1997) An improved methodology for characterizing atmospheric boundary layer turbulence and dispersion. PhD thesis, University of Illinois
- Cai XM (2012) Effects of wall heating on flow characteristics in a street canyon. *Boundary-Layer Meteorol* 142(3):443–467
- Cheng W, Liu CH (2011) Large-eddy simulation of turbulent transports in urban street canyons in different thermal stabilities. *J Wind Eng Ind Aerodyn* 99(4):434–442
- Christen A, van Gorsel E, Vogt R (2007) Coherent structures in urban roughness sublayer turbulence. *Int J Climatol* 27(14):1955–1968
- Coceal O, Thomas TG, Castro IP, Belcher SE (2006) Mean flow and turbulence statistics over groups of urban-like cubical obstacles. *Boundary-Layer Meteorol* 121(3):491–519
- Coceal O, Dobre A, Thomas TG (2007a) Unsteady dynamics and organized structures from DNS over an idealized building canopy. *Int J Climatol* 27(14):1943–1953
- Coceal O, Thomas TG, Belcher SE (2007b) Spatial variability of flow statistics within regular building arrays. *Boundary-Layer Meteorol* 125(3):537–552
- Deardorff JW (1980) Stratocumulus-capped mixed layers derived from a three-dimensional model. *Boundary-Layer Meteorol* 18(4):495–527
- Gousseau P, Blocken B, Stathopoulos T, Van Heijst G (2011) CFD simulation of near-field pollutant dispersion on a high-resolution grid: a case study by LES and RANS for a building group in downtown montreal. *Atmos Environ* 45(2):428–438
- Hillel D (1982) Introduction to soil physics. Academic, New York, pp 364
- Inagaki A, Castillo MCL, Yamashita Y, Kanda M, Takimoto H (2012) Large-eddy simulation of coherent flow structures within a cubical canopy. *Boundary-Layer Meteorol* 142(2):207–222
- Kim JJ, Baik JJ (1999) A numerical study of thermal effects on flow and pollutant dispersion in urban street canyons. *J Appl Meteorol* 38(9):1249–1261
- Kim JJ, Baik JJ (2001) Urban street-canyon flows with bottom heating. *Atmos Environ* 35(20):3395–3404
- Kovar-Panskus A, Moulinneuf L, Savory E, Abdelqari A, Sini JF, Rosant JM, Robins A, Toy N (2002) A wind tunnel investigation of the influence of solar-induced wall-heating on the flow regime within a simulated urban street canyon. *Water Air Soil Pollut* 2(5–6):555–571
- Krayenhoff ES, Voogt JA (2007) A microscale three-dimensional urban energy balance model for studying surface temperatures. *Boundary-Layer Meteorol* 123(3):433–461
- Letzel MO, Krane M, Raasch S (2008) High resolution urban large-eddy simulation studies from street canyon to neighbourhood scale. *Atmos Environ* 42(38):8770–8784
- Li XX, Britter RE, Koh TY, Norford LK, Liu CH, Entekhabi D, Leung DY (2010) Large-eddy simulation of flow and pollutant transport in urban street canyons with ground heating. *Boundary-Layer Meteorol* 137(2):187–204
- Maronga B, Gryscha M, Heinze R, Hoffmann F, Kanani-Sühring F, Keck M, Ketelsen K, Letzel M, Sühring M, Raasch S (2015) The parallelized large-eddy simulation model (PALM) version 4.0 for atmospheric and oceanic flows: model formulation, recent developments, and future perspectives. *Geosci Model Dev Discuss* 8(2015), Nr 2, S 1539–1637
- Meroney RN, Pavageau M, Rafailidis S, Schatzmann M (1996) Study of line source characteristics for 2-D physical modelling of pollutant dispersion in street canyons. *J Wind Eng Ind Aerodyn* 62(1):37–56
- Michioka T, Sato A, Takimoto H, Kanda M (2011) Large-eddy simulation for the mechanism of pollutant removal from a two-dimensional street canyon. *Boundary-Layer Meteorol* 138(2):195–213
- Nakamura Y, Oke TR (1988) Wind, temperature and stability conditions in an east–west oriented urban canyon. *Atmos Environ* (1967) 22(12):2691–2700
- Nazarian N, Kleissl J (2015) CFD simulation of an idealized urban environment: thermal effects of geometrical characteristics and surface materials. *Urban Clim* 12:141–159
- Nazarian N, Kleissl J (2016) Realistic solar heating in urban areas: air exchange and street-canyon ventilation. *Build Environ* 95:75–93
- Park SB, Baik JJ, Raasch S, Letzel MO (2012) A large-eddy simulation study of thermal effects on turbulent flow and dispersion in and above a street canyon. *J Appl Meteorol Clim* 51(5):829–841

- Pedersen C, Liesen R, Strand R, Fisher D, Dong L, Ellis P (2001) A toolkit for building load calculations; exterior heat balance. American Society of Heating, Refrigerating and Air-Conditioning Engineers, Inc. (ASHRAE), Building Systems Laboratory, New York
- Piacsek SA, Williams GP (1970) Conservation properties of convection difference schemes. *J Comput Phys* 6(3):392–405
- Qu Y, Milliez M, Musson-Genon L, Carissimo B (2012) Numerical study of the thermal effects of buildings on low-speed airflow taking into account 3D atmospheric radiation in urban canopy. *J Wind Eng Ind Aerodyn* 104:474–483
- Raasch S, Schröter M (2001) PALM-a large-eddy simulation model performing on massively parallel computers. *Meteorol Z* 10(5):363–372
- Raupach MR, Thom AS (1981) Turbulence in and above plant canopies. *Annu Rev Fluid Mech* 13(1):97–129
- Raupach MR, Shaw RH (1982) Averaging procedures for flow within vegetation canopies. *Boundary-Layer Meteorol* 22(1):79–90
- Salim SM, Buccolieri R, Chan A, Di Sabatino S (2011) Numerical simulation of atmospheric pollutant dispersion in an urban street canyon: Comparison between RANS and LES. *J Wind Eng Ind Aerodyn* 99(2):103–113
- Salizzoni P, Soulhac L, Mejean P (2009) Street canyon ventilation and atmospheric turbulence. *Atmos Environ* 43(32):5056–5067
- Santiago J, Krayenhoff E, Martilli A (2014) Flow simulations for simplified urban configurations with microscale distributions of surface thermal forcing. *Urban Clim* 9:115–133
- Shaw RH, Tavangar J, Ward DP (1983) Structure of the Reynolds stress in a canopy layer. *J Appl Meteorol Clim* 22(11):1922–1931
- Sini JF, Anquetin S, Mestayer PG (1996) Pollutant dispersion and thermal effects in urban street canyons. *Atmos Environ* 30(15):2659–2677
- Stewart ID, Oke TR (2012) Local climate zones for urban temperature studies. *Bull Am Meteorol Soc* 93(12):1879–1900
- Tan Z, Dong J, Xiao Y, Tu J (2015) A numerical study of diurnally varying surface temperature on flow patterns and pollutant dispersion in street canyons. *Atmos Environ* 104:217–227
- Uehara K, Murakami S, Oikawa S, Wakamatsu S (2000) Wind tunnel experiments on how thermal stratification affects flow in and above urban street canyons. *Atmos Environ* 34(10):1553–1562
- Wallace JM, Eckelmann H, Brodkey RS (1972) The wall region in turbulent shear flow. *J Fluid Mech* 54(01):39–48
- Willmarth W, Lu S (1972) Structure of the Reynolds stress near the wall. *J Fluid Mech* 55(01):65–92
- Xie ZT, Castro IP (2009) Large-eddy simulation for flow and dispersion in urban streets. *Atmos Environ* 43(13):2174–2185
- Xie X, Liu CH, Leung DY, Leung MK (2006) Characteristics of air exchange in a street canyon with ground heating. *Atmos Environ* 40(33):6396–6409
- Xie X, Liu CH, Leung DY (2007) Impact of building facades and ground heating on wind flow and pollutant transport in street canyons. *Atmos Environ* 41(39):9030–9049
- Yaghoobian N, Kleissl J (2012) An indoor-outdoor building energy simulator to study urban modification effects on building energy use—model description and validation. *Energy Build* 54:407–417
- Yaghoobian N, Kleissl J, Paw UKT (2014) An improved three-dimensional simulation of the diurnally varying street-canyon flow. *Boundary-Layer Meteorol* 153(2):251–276
- Zmeureanu R, Fazio P, Haghghat F (1987) Analytical and inter-program validation of a building thermal model. *Energy Build* 10(2):121–133